ISSN 1392–1207. MECHANIKA. 2022 Volume 28(2): 121–129

# Development of an Independent Front Suspension for Truck Tractors

**Mehmet Murat TOPAÇ*, Can OLGUNER**, Egemen BAHAR*****
**Department of Mechanical Engineering, Dokuz Eylül University, 35397, Izmir, Turkey, E-mail: murat.topac@deu.edu.tr*
***The Graduate School of Natural and Applied Sciences, Dokuz Eylül University, 35397, Izmir, Turkey, E-mail: can.olguner@ogr.fbe.deu.edu.tr*
****The Graduate School of Natural and Applied Sciences, Dokuz Eylül University, 35397, Izmir, Turkey, E-mail: egemen.bahar@ogr.fbe.deu.edu.tr*

crossref http://dx.doi.org/10.5755/j02.mech.29092

## 1. Introduction

Due to their load-carrying capacity and economically affordable nature, rigid axles have a large area of use, especially in heavy commercial vehicle applications. The change in track width and camber angle as a result of vehicle body motions during the service is more significant for heavy commercial vehicles when compared to personal vehicles. The smaller these parameters change, the lower tyre wear and rolling resistance are observed; and, as a result of the latter one, fuel economy is improved as well. Therefore, the vehicle serves more economically throughout its service life. Although the rigid axle suspension systems help to obtain benefits in those mentioned above to a large extent, it also brings along problems regarding the vibration transfer and as a result of that noise disturbance [1, 2]. In addition, larger unsprung mass in rigid axle suspension systems compared to those in independent suspension systems influences the road-tyre contact, and consequently the driving dynamics in a negative way [3, 4]. In order to reduce the effects of this problem, keeping the unsprung mass as low as possible became one of the most essential goals in the design of vehicle suspension systems. With an increasing rate, the heavy commercial vehicle manufacturers started using double-wishbone type independent suspension system for the front axle of buses and trucks, as a consequence of the comfort and control concerns [5]. Aside from these, another advantage of the independent suspension systems can be given as the more effective usage of the vehicle interior volume [6].

In this study, development and experimental validation stages of an independent front suspension system, which is considered to be used in the front axle of a semi-trailer truck, is given. The approximate mass fraction of the truck is given in Fig. 1. From the diagram, it is understood that a slightly higher than a quarter portion of the total vehicle mass stands for the suspension system in that kind of vehicle. The methodology used is summarised in Fig. 2. In the first part of the study, a semi-truck model with a rigid axle suspension system is considered and useful volume, as well as the approximate kinematic connection points are determined, considering design restrictions. Using MSC.Adams® Multibody Dynamics *(MBD)* commercial software, the initial kinematic model of the system is created and the variation range of the kinematic parameters depending on the vertical wheel motion is calculated. In the next stage, suspension system hardpoints that allow the minimum possible change in the camber angle and track width during the vertical wheel motion are determined with the help of a multi-objective optimisation module.

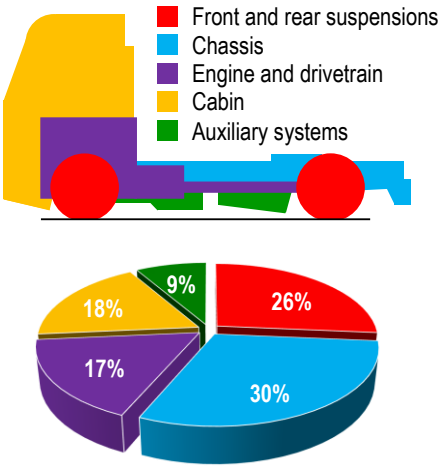


Fig. 1 Approximate mass fraction for a truck tractor

The obtained suspension geometry is then used to carry out matrix algebra-based force analyses and consequently the applied forces for suspension system elements are determined as per units. Using the corresponding forces, the pre-dimensioning and mechanical design were made for the structural elements. For the selected critical load conditions, the Finite Element Method *(FEM)* were carried out for the complete suspension system and stress concentrated regions were detected. In order to overcome possible failure during the service, some design improvements were applied to the relevant regions. At the final part of the study, produced prototypes were subjected to lateral and vertical fatigue tests with the help of a hydraulic experimental set-up, in order to simulate real-life working conditions of the vehicle. Throughout the tests, previously collected road data for equivalent vehicles with similar carrying capacity are employed. As a result of this study, it is seen that the designed suspension system does not experience any static or fatigue failure.

To the authors' best, there are some studies regarding the kinematic optimisation and mechanical improvements of some structural elements in suspension systems are available in the literature. Yamanka et al. Developed a genetic algorithm-based optimisation method for independent suspension systems [7]. Hwang et al. assessed a double-wishbone type independent suspension system from a kinematic perspective and obtained optimal positions of connecting points by means of a genetic algorithm-based multi-objective optimisation method [8]. Sancibrian et. al. performed the kinematic design of a similar suspension system using a multi-objective dimensional synthesis [9]. Arikere et al. used a genetic algorithm based *NSGA-II* optimisation

algorithm to reduce the toe and camber angle change [10]. Zhang et al. employed a genetic algorithm based Isight-*FD* algorithm to optimise suspension system parameters [11]. Mechanical design optimisation related studies are also available in the literature. Heo et al. carried out a study using the meta-model approach for the shape optimisation of a lower wishbone that is used in a personal vehicle [12]. Although they are not as frequently encountered as the others, there are also some works that focus on the independent suspension systems for heavy commercial vehicles. Some of these are carried out by Yarmohamadi and Berbyuk, in which the kinematics and dynamics of relevant systems are evaluated employing analytical expressions and simulations [13, 14].

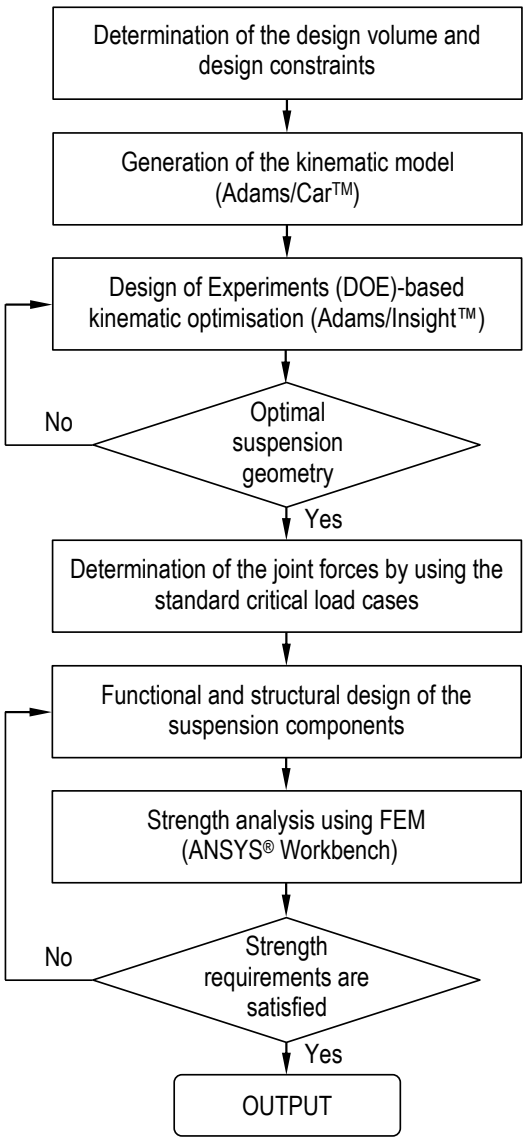


Fig. 2 Workflow for the suspension system design

The given papers focused mainly on the different aspects of the independent suspension systems, rather than investigating the design of the system as a whole. Hence, this study aims to contribute to the literature by presenting a methodology for an independent suspension system design.

## 2. Design volume

The design volume and the existing rigid suspension system of the truck tractor are given in Fig. 3. Here, the ground clearance *h* is constrained by the axle beam *2* and track rod *3*. Due to its compact structure, hydropneumatic suspension element is utilised in design. As a result of avoiding not only the axle beam but also the leaf springs *1*, the effective design volume increases significantly.

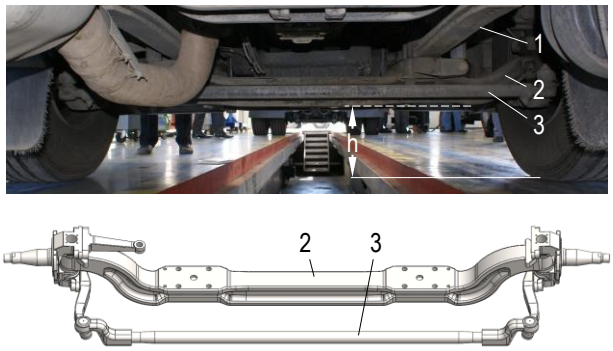


Fig. 3 Rigid front suspension of the truck tractor

## 3. Kinematic design and optimisation

The main kinematic parameters, which are considered in double wishbone-type independent suspension system design, are summarised in Fig. 4, a. The main objective of the optimum kinematic design study is the determination of suspension geometry, which satisfies the minimum change in camber angle $\sigma$ and track width $s_{RV}$ during the vertical motion of the wheel. The allowable design areas for the hardpoints are also given in Fig. 4, a. as well. The middle point of front track width $O_1$ is taken as the location of the reference coordinate system ($X_1$, $Y_1$, $Z_1$). Here, e.g. $\zeta$ is the position constraint of joint *C* in $Y_1$ direction. Determinative factors for the proper control arm hardpoint positions *C* and *D* are the design volumes of steel wheel and brake disc, sufficient volume for spring assembly and avoiding high bending loads on stub axle. Regarding *A* and *E* joints, through which the control arms are connected to subframe, the factors such as penetration of upper control arm to vehicle frame during a bump motion, ground clearance and the roll centre position, are considered. It is necessary that the roll centre is as close as possible to the ground during driving, in order to keep the change in camber angle and track width as small as possible [15]. In addition, the greater length *c* result in the smaller joint forces for lateral tyre loads [16]. In the model vehicle, front axle ground clearance *h* is determined by the axle beam. In this study, ground clearance of the model vehicle is used as a design constraint during optimisation stage. In order to determine the optimum locations of hardpoints, Design of Experiments – Response Surface Methodology (*DOE – RSM*) approach is employed. The optimisation is carried out using Adams/Insight™ software. The broad theoretical background of this well-known method is given in [17] and [18], whereas, a detailed application for a multi-link steering mechanism of a bus can be found in [19]. To determine the proper design points, Central Composite Design (*CCD*) is applied, which offered as an option in the definition of design table of Adams/Insight™ software [20, 21].

Firstly, vertical wheel displacement simulation is applied to initial design model with maximum wheel travel range of $Z_R = \pm 100$ mm. Then, wheel camber $\sigma$ and front track $s_{RV}$ are introduced to the software as design objectives. The maximum absolute values of kinematic parameters, which are obtained from the first analysis and the initial

kinematic design, are transferred to Adams/Insight™ software. Considering design constraints and objectives, the highest and lowest physical values of selected factors are introduced to the software. Analysis type is selected as Design of Experiments (*DOE*)–Response Surface Methodology (*RSM*). Using the results of consecutive kinematic analyses, which are applied to design candidates which are created using design points selected by *CCD* approach, design matrix is generated. Finally, with the help of the regression model that is created using design matrix, optimal locations for the connection points are determined. The variation ranges of factors are selected as ±30 mm for $A_Y$ and $E_Y$, and ±15 mm for the remaining, taking the design constraints into account. The maximum, minimum and optimal values of the factors, as well as their highest values within $Z_R$= ± 100 mm vertical displacement range, are given in Table 1. The "Maximum" and "Minimum" rows given in Table 1 represent the design candidates, which result in highest and lowest output values within the range of $Z_R$= ± 100 mm, among generated design samples, respectively. The "Optimal" row shows the maximum absolute values of the parameter, which is selected as objective, by using determined optimal geometry, within the relevant vertical displacement range.

Table 1

Variation ranges and optimal values of camber and half-track for left front wheel

| Parameter | $\sigma$, ° | $\Delta s_{RV}$ / 2, mm |
|---|---|---|
| Target | Minimum | Minimum |
| Minimum | 0.409 | 16.36 |
| Maximum | 4.472 | 34.057 |
| Optimal | 1.838 | 17.789 |

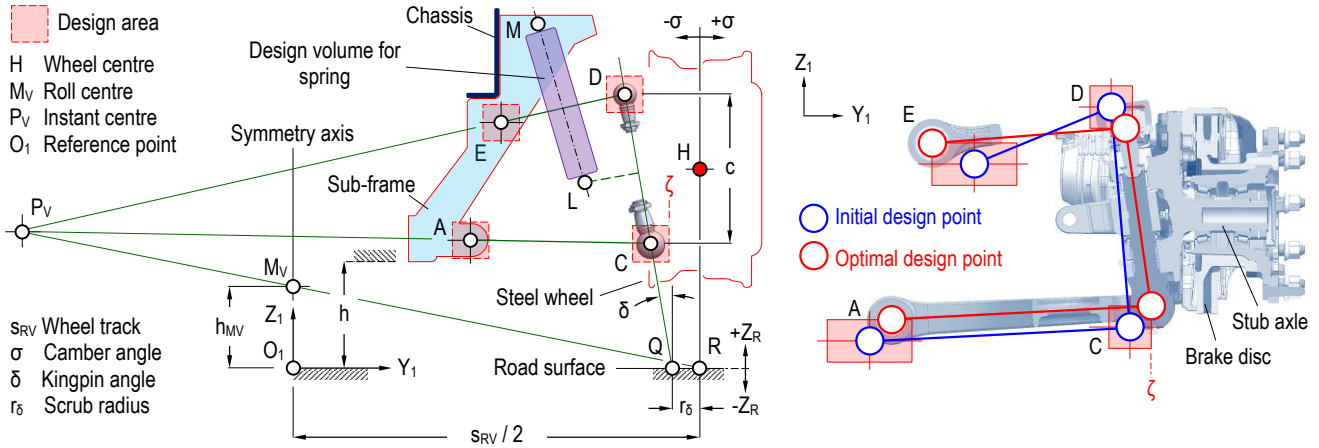


a b

Fig. 4 a) Kinematic parameters and design constraints (schematic); b) Comparison of initial and optimal model geometries

The optimal kinematic model, which is generated using the connection points that are obtained as result of the optimisation process, is also compared with the initial model in Fig. 4, b. The variations of kinematic parameters, depending on the vertical wheel travel of tyre contact point *R*, are given in Fig. 5 for initial and optimised suspension geometries. As a general design rule, it is required that, the change in track width of steered wheels does not exceed 25 mm for a total 80 mm of wheel travel ($Z_R$= ±40 mm) [22]. When Fig. 5 is examined, it is seen that the design objective is met. It is obtained that, the changes in camber angle and track width are reduced by 30% and 57%, respectively.

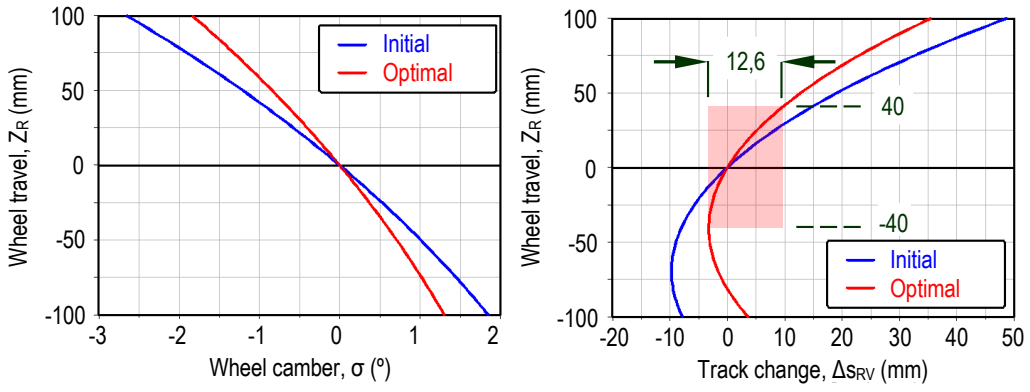


a b

Fig. 5 Variations of kinematic parameters as functions of $Z_R$: a. $\sigma$ and b. $s_{RV}$

## 4. Joint forces

It can be assumed that, in the most general case, a non-driven vehicle wheel is subjected to vertical *P*, lateral *S* and braking *B* forces. These forces, which are considered as acting through wheel contact point *R*, are carried by the springs and other suspension system elements, depending on the loading type. Fig. 6 shows the forces that act upon suspension system elements schematically. Here, $R_D$ is the dynamic radius of the wheel.

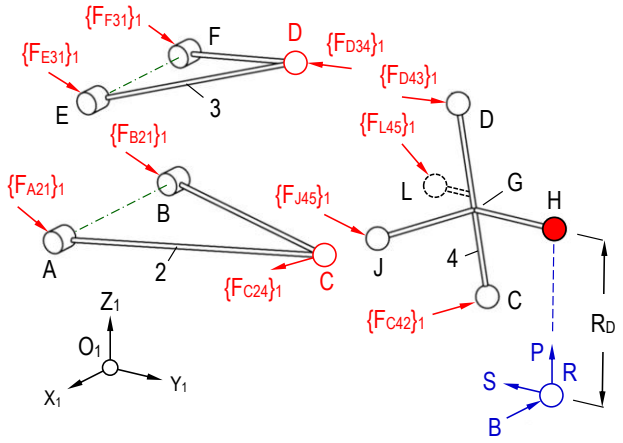


Fig. 6 Reaction forces on the suspension parts

The notations in the figure are arranged such that, for example, $\{F_{C24}\}_1$ represents the force $F$ which is transferred from wheel carrier *4* to lower control arm *2* through joint *C*, and expressed with respect to coordinate system *1*, $O_1$. Furthermore, the total force equilibrium $\Sigma\{F_2\}_1$, and as an example, the moment equilibrium about the point *C* $\Sigma\{M_{C2}\}_1$ can be expressed in matrix form with respect to reference coordinate system $O_1$, by neglecting inertial effects [23]:

$$\sum\{F_2\}_1 = \{0\}_1 , \tag{1}$$

$$\{F_{A21}\}_1 + \{F_{B21}\}_1 + \{F_{C24}\}_1 = \{0\}_1 , \tag{2}$$

$$\begin{bmatrix} F_{A21x} \\ F_{A21y} \\ F_{A21z} \end{bmatrix} + \begin{bmatrix} F_{B21x} \\ F_{B21y} \\ F_{B21z} \end{bmatrix} + \begin{bmatrix} F_{C24x} \\ F_{C24y} \\ F_{C24z} \end{bmatrix} = \begin{bmatrix} 0 \\ 0 \\ 0 \end{bmatrix}, \tag{3}$$

$$\sum\{M_{C2}\}_1 = \{0\}_1 , \tag{4}$$

$$\{R_{AC}\}_1 \times \{F_{A21}\}_1 \times \{R_{BC}\}_1 \times \{F_{B21}\}_1 = \{0\}_1 , \tag{5}$$

here: $\{R_{AC}\}_1$ and $\{R_{BC}\}_1$ are skew-symmetric position matrices which can be written with respect to reference coordinate system as:

$$\{R_{AC}\}_1 = \begin{bmatrix} 0 & -R_{ACz} & R_{ACy} \\ R_{ACz} & 0 & -R_{ACx} \\ -R_{ACy} & R_{ACx} & 0 \end{bmatrix}, \tag{6}$$

$$\{R_{BC}\}_1 = \begin{bmatrix} 0 & -R_{BCz} & R_{BCy} \\ R_{BCz} & 0 & -R_{BCx} \\ -R_{BCy} & R_{BCx} & 0 \end{bmatrix}. \tag{7}$$

Exact values of the matrix elements were determined in the previous chapter by using *DOE*. The matrix solution of the equation system which is generated by spanning the notation above to all suspension elements yields to determination of joint forces. Details of this procedure can be found in [23]. In order to determine the ratios of upper and lower joint forces of kingpin, which can possibly occur during vertical and lateral loading, a 1*g* load is applied from wheel contact point *R*, which is shown along with the model given in Fig. 6, in $Y_1$ and $Z_1$ directions separately. The components of the reaction forces of joints *C* and *D* are given comparatively in Fig. 7 where, maximum force value is represented as 1.0.

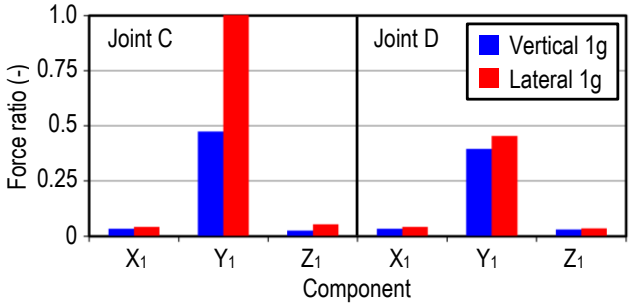


Fig. 7 Comparison of the reaction force components

## 5. Mechanical design and optimisation

The force analyses revealed that, especially under lateral loading, joint *C* of lower control arm is forced approximately 2.2 times of the upper control arm joint *D*. Therefore, it is suggested that, the connection of lower control arm should be made using a revolute joint *R* instead of a spherical joint *S*. The kinematic model of double wishbone independent suspension system which is designed within the scope of this study is shown in Fig. 8.

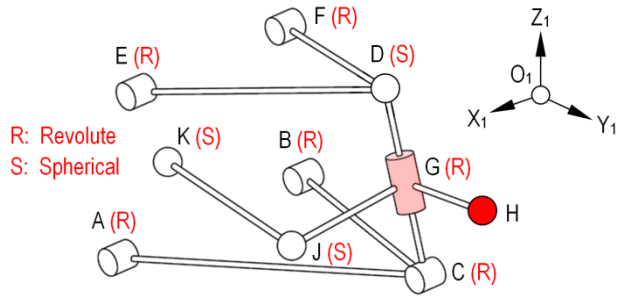


Fig. 8 Kinematic model of the *IFS*

In this design, the wheel carrier is mounted on the kingpin with a revolute joint *G*. The steering angle of the wheel is controlled by tie rod *JK* which is connected to the rod *JG* of the steering knuckle with a spherical joint. During the design process, it is considered that, wishbones are not forced under extra bending loads where possible. As a result, the ball joint of upper wishbone, which carries a smaller load, is located in such a way that the spherical part is mounted to the wishbone [24]. Moreover, the spring is mounted on kingpin instead of the lower wishbone. By this way it becomes possible to obtain a lighter wishbone structure. General view of the suspension system is shown in Fig. 9. The suspension knuckle axle is steered through kingpin, similar to conventional double wishbone suspension systems. However, in this design, the connection between lower wishbone and kingpin is made using a revolute joint. The bearing on kingpin carries the connection pin for lower wishbone [25].

Throughout the analyses which are carried out as a part of the mechanical strength validation, the standard quasi-static load conditions that are given in literature are applied [6]. In this study, besides the 1*g* static loading *1*, the most critical three among the 16 relevant load types are selected, namely, the 3*g* vertical bump *2*, brake in turn *5*, and

cornering *6* cases. The corresponding gravitational acceleration *g* components are given in Table 2. The relevant components may be considered as constants that are used for the forces which act through wheel contact point in static condition.

Table 2

Selected standard load cases according to [6]

| Standard load case | Acceleration in *g* | | |
|---|---|---|---|
| | *X* | *Y* | *Z* |
| 1. Static load | 0,00 | 0,00 | 1,00 |
| 2. Vertical bump (3*g*) | 0,00 | 0,00 | 3,00 |
| 5. Cornering | 0,00 | 1,25 | 1,00 |
| 6. Brake in turn | 0,75 | 0,75 | 1,00 |

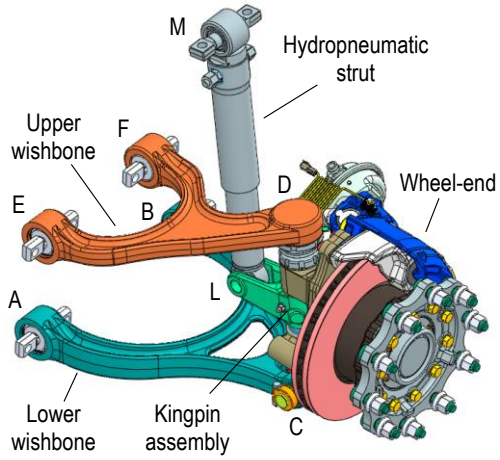


Fig. 9 General view of the truck tractor *IFS*

The generated parametric assembly model is exported to commercial *FE* software ANSYS® Workbench in order to apply stress analyses. During the analyses, the Young's Modulus *E* is taken as 200 GPa and 170 GPa for steel and cast iron, respectively. The Poisson's ratio is assumed as $\upsilon$= 0.3 (-). The weight of the suspension system is approximately 6.2% of the maximum design load that acts through the wheel contact point. Although they are relatively low compared to service loads, the masses of the components are also considered throughout the analyses. Under vertical loading condition, von Mises stress distribution that is obtained for the whole system is shown in Fig. 10, as well as the critical regions *R*1, *R*2 and *R*3.

Due to its functions of carrying the spring force and wheel guidance during steering, kingpin is the most crucial structural element of the system. The ratios of maximum von Mises stresses $\sigma_V$ that are observed in the critical regions to the yielding stress $\sigma_y$ of pin material are shown in Fig. 11 for the four assessed load cases. The assessment is made for three critical regions, namely, kingpin body *a*, shoulder fillet *b*, and the inner surface of the lower joint *c* in which roller bearings are mounted. It is seen that safety condition is satisfied for the examined regions.

Another critical structural element of the suspension system is the upper wishbone. This component is mainly forced to bending under vertical and lateral wheel forces during service. Torsional effects which may occur as a result of braking should also be considered. For this reason, the cross-section of the upper wishbone is chosen as I-type which exhibits resistance against both loading types. It was also formed, such as, compressive stresses occur at *R1* under vertical bump and braking loads. Even though it is subjected to lower forces during service when compared to lower wishbone (Fig. 7), as a result of its curved shape, stress concentrated regions are observed on this part as seen in Fig. 12. These stress concentrations are observed along an arc which is defined by $\xi$ angle, and more locally, in region *M*. It is seen that, the highest stress which emerges as a result of load case 2 (3*g*). The relevant stress mainly exhibits compressive characteristic in bump mode. Orientation of the compressive principal stress $\sigma_P$ for this condition is also seen in Fig 10. In order to reduce the stress concentration in the critical area, a shape optimisation study is also made. For that means, reinforcement of original I-section of wishbone (blue) with a rib *c* is considered as shown in Fig. 13. Therefore, shear web thickness and rib height, which are given as $P_1$ and $P_2$, respectively, are specified as design parameters of the geometry.

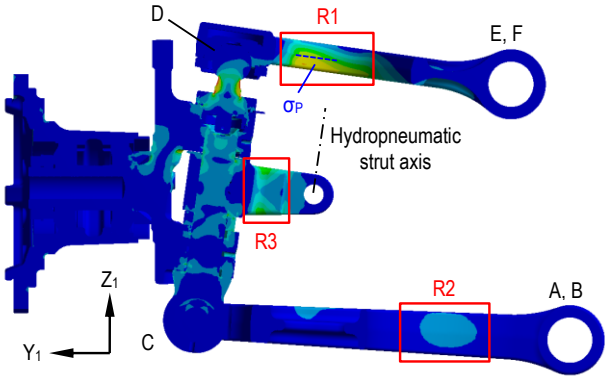


Fig. 10 Critical regions on the *IFS FE* model

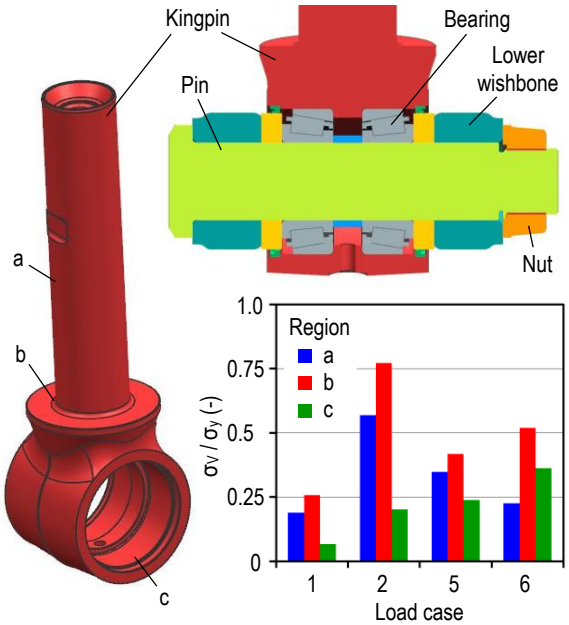


Fig. 11 $\sigma_V/\sigma_y$ ratios on kingpin for selected load cases

In optimisation process, *CCD* is also used. The design targets are assigned as the minimum stress and minimum mass increase of the optimal part. When Fig. 7 is reviewed, it is seen that, the vertical load that acts through wheel contact point is carried by the wishbones, mainly along the lateral axis ($\pm Y_1$). The reason for this is that the springs used in the suspension system are not connected to wishbones but to kingpins, and as a result, no large force components along vertical or longitudinal direction emerge in *C* and *D* joints. Thus, the optimisation study is made using

those forces which are considered that they act on ($X_1$-$Y_1$) plane. The upper and lower bounds of input parameters are specified by taking the manufacturing method of the part into account. During the structural optimisation, values of $P_1$ and $P_2$ varied between the 0.75-1.67 and 0.89-1.16 multiples of their initial values $P_{1,0}$ and $P_{2,0}$, respectively.

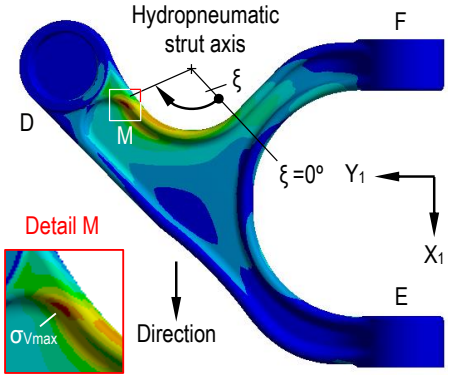


Fig. 12 Stress concentration on the upper wishbone

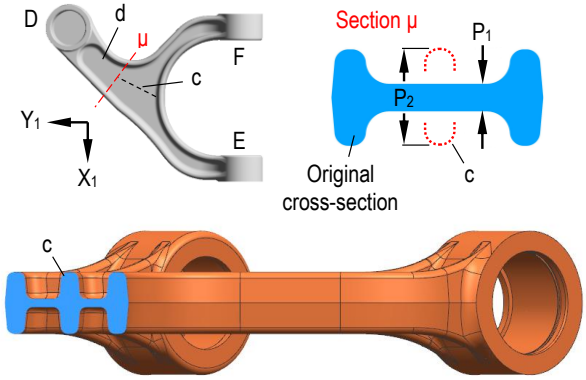


Fig. 13 Design parameters for the structural optimisation of the upper wishbone

In Figs.14, a and b, the changes in the maximum von Mises stresses on critical region which occur due to cornering and braking loading types are shown within the selected range for them. Here, *L* is the initial design point. As expected, raise in both parameters aid reducing the stress concentration. The optimised structure of the upper wishbone is also seen in Fig. 13. The optimization study shows that, the rib could solely reduce the von Mises stress in the critical region by up to 21.1%. In addition to rib *c*, reinforcement is also applied to that region of the upper wishbone which is termed as *d*.

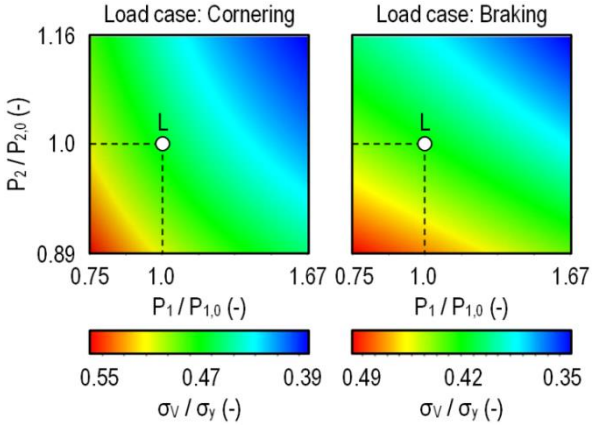


Fig. 14 Response surfaces: a) cornering; b) braking

## 6. Prototyping and bench tests

Since the vehicle suspensions are evaluated as safety systems, their fatigue behaviours should be determined experimentally. For that purpose, two prototypes of the final suspension design were produced for bench tests. The general view of the test prototype is seen in Fig. 15.

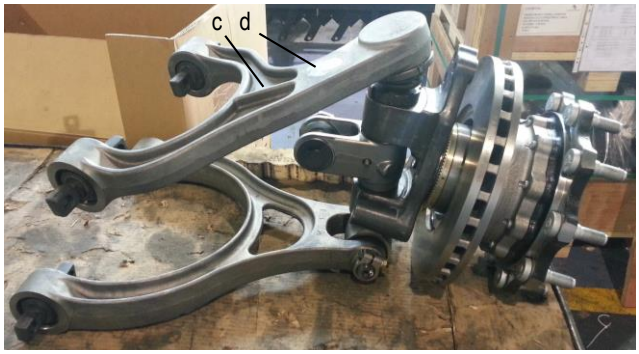


Fig. 15 Test prototype of the truck tractor *IFS*

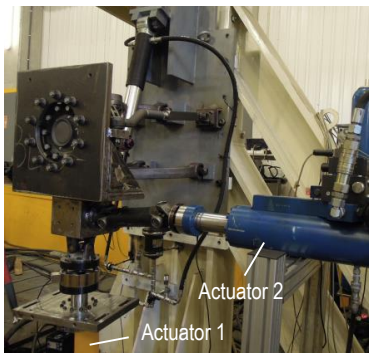


a

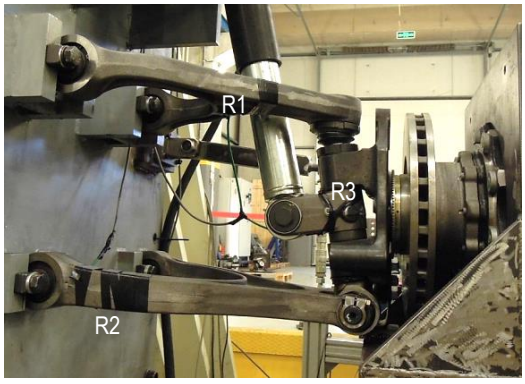


b

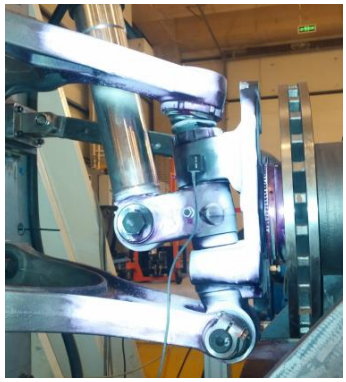

c

Fig. 16 a) Bench test setup; b) Strain measurement points on the prototype; c) Dye penetrant inspection

Durability tests were performed in *OTAM*, Automotive Technology Research Centre in Istanbul, Turkey. The experimental setup is also shown in Fig. 16, a. Some details are not given due to the confidetiality policy of *OTAM*. The forces that are applied on the suspension prototypes are produced by actuators 1 and 2. Those which are produced by actuator 1 are carried by the hydropneumatic suspension unit. The bench tests were made in such way that the vertical motion of wheel centre is limited by $Z_R$= ± 100 mm. Strain values of three critical regions on which stress concentrations are observed during finite element analyses, were measured with strain gauges. By this way, variation ranges of stresses which are likely to occur under dynamic loads were obtained in relevant areas (Fig.16, b). Orientations of the strain gauges were determined in accordance to the results of *FE* analyses. In order to examine whether any structural failure starts in one of the components of the system, the procedure was paused in certain intervals and a non-destructive failure test was applied using penetrant liquid as it is given in Fig. 16, c. At the first step of the tests, four times of nominal design load was applied to the prototype 1 vertically with actuator 1. During this stage, no structural failure was observed on the suspension prototype.

In the following step, the behaviour of the suspension system under the dynamic loads which emerge under real-life driving conditions was examined. To this end, the load characteristics that are produced considering the road data of a similar weight category vehicle were applied to prototype 2.

The fatigue tests were carried out in three substages overall. Firstly, during driving on a rough asphalt road while fully loaded, the dynamic characteristics of stresses that are seen in the critical regions of suspension system were examined. As an example, the vertical acceleration of wheel-end is given in Fig. 17. This acceleration fluctuates between the instantaneous maximum values of -6,5*g* / +6,7*g*.

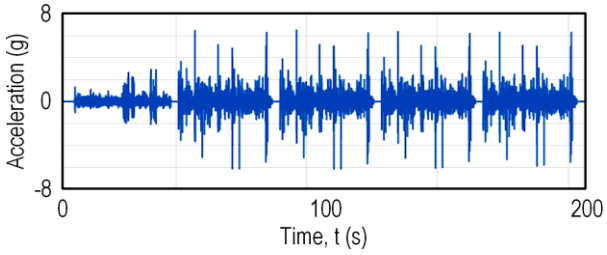


Fig. 17 Vertical acceleration characteristic for rough asphalt condition

The ratios of principal stresses which are observed on critical regions *R*1, *R*2, and *R*3 throughout the vertical fatigue tests to the yield stresses of component materials are shown in Fig. 18. It is seen that the peak values of the stresses remain in considerably low levels. Secondly, the suspension prototype was tested under a cyclic test load that approximately corresponds to 2.5 *g* vertical acceleration within ±70 mm sinusoidal stroke. Note that, in open literature, 2.25 *g* is accepted as appropriate for durability evaluations [6]. The change in principal stress ratio for *R*1 region is seen in Fig. 19 as example. The maximum stress ratio becomes 0.264. Here, compressive stress dominates the critical region at bump mode. In *R*2 and *R*3 regions, it is observed that the stress ratios do not exceed 0.117 and 0.281, respectively. Stresses on *R*2 and *R*3 have tensile nature.

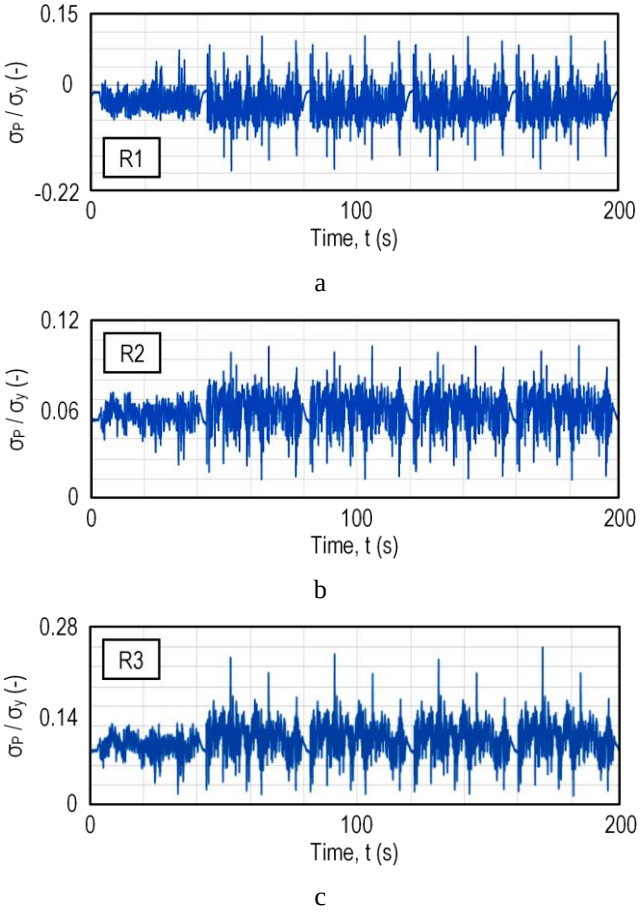


Fig. 18 Time-dependent stress ratios measured at critical regions: a) *R*1; b) *R*2; c) *R*3

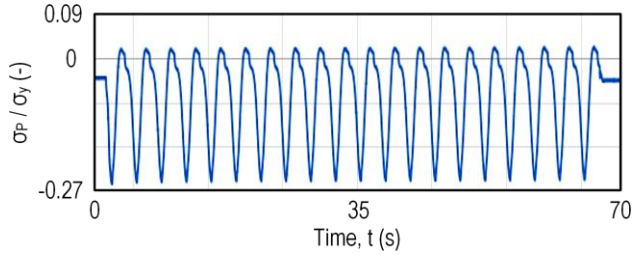


Fig. 19 Time-dependent stress ratio measured at *R*1 under sinusoidal loading

At the final step of validation study, the effects of braking forces on the system are evaluated. Therefore, a force that corresponds to 0.58 *g* braking acceleration is applied on the system using actuator 2. During braking, it is observed that the critical region of upper wishbone *R*1 works under compressive stress. The maximum stress ratios on regions *R*1, *R*2 and *R*3 are -0.11, 0.074 and 0.344, respectively.

Throughout the bench test procedures, no means of failures such as overload or fatigue are witnessed on the system.

## 7. Conclusions

In this study, development and validation stages of a double wishbone-type front suspension system for articulated heavy commercial vehicles are presented. In that regard, a design methodology which combines different approaches such as *DOE – RSM*, *MBS* and *FEM* is summarised. Some results drawn from this study are summarised

below:

- As a result of the kinematic optimisation study, in which *MBS* and *DOE* approaches are utilised, final suspension geometry satisfies the condition of $\Delta s_{RV} \leq 20$ mm for ±40 mm vertical wheel travel.
- According to the results obtained from the *FE* analyses of the full suspension model, the most critical load case from mechanical strength perspective is specified as 3 *g* vertical bump (2). Analyses showed that the critical components of the suspension satisfy the strength conditions for this case.
- A series of bench tests including various loading scenarios were applied to the suspension prototype. Stress types observed in *FE* analyses agree with those obtained from bench tests. No structural failure was observed during these tests.
- The designed suspension system (pair) is about 31 % lighter compared to a rigid axle suspension system with same carrying capacity excluding tyres and steel wheels.

## Acknowledgement

First author is grateful to the Ministry of Science, Industry and Technology of Republic of Turkey due to their support for this study within the scope of Industrial Theses (SAN-TEZ) program (Grant number: 0281.STZ.2013-2). The authors also wish to thank Ege Endüstri ve Ticaret A.Ş., the project partner, for technical and financial support.

Some results presented in the Section 5 are extracted from the MSc thesis of the second author [25] which was supervised by the first author. The authors are also thankful to Mr. A. Özel, The General Manager, Mr. O. Balcı, The R&D Manager, Mr. A. Güler, The R&D Chief and Mr. A. Yenice, R&D engineer at Ege Endüstri ve Ticaret A.Ş. in Izmir, Turkey, Mr. S.V. Bayraktar, Mr. Ş.S. Ersolmaz, Senior Management of Automotive Technology Research Centre *(OTAM)* in Istanbul, Turkey, and Prof. (Emeritus) N. S. Kuralay. Authors also acknowledge the licensed software support of BİAS Engineering in Istanbul, Turkey.

## References

1. **Bramberger, R.; Eichlseder, W.** 1998. Investigations of Independent Suspension on Trucks. International Truck & Bus. Meeting & Exposition. SAE 982843. http://dx.doi.org/10.4271/982843.
2. **Fleuren, P. W.** 2009. Independent Front Suspensions on Trucks: Ride Comfort Analysis and Improvements. Eindhoven University of Technology, Department of Mechanical Engineering, Dynamics and Control Group. DTC Report No: 2009.065. 91 p.
3. **Gillespie, T. D.** 1992. Fundamentals of Vehicle Dynamics. Warrendale, PA: Society of Automotive Engineers, Inc. 470 p.
4. **Gysen, B. L. J.; Paulides, J. J. H.; Janssen, J. L. G.; Lomonova, E. A.** 2010. Active electromagnetic suspension system for improved vehicle dynamics, IEEE Transactions on Vehicular Technology 59(3) :1156-1163. http://dx.doi.org/10.1109/VPPC.2008.4677555.
5. **Timoney, E.; Timoney S.** 2003. A review of the development of independent suspension for heavy vehicles, 2003 SAE International Truck and Bus Meeting and Exhibition. SAE Technical Paper 2003-01-3433. http://dx.doi.org/10.4271/2003-01-3433.
6. **Heißing, B; Ersoy, M; Gies, S.** (Hrsg.). 2011. Fahrwerkhandbuch, Wiesbaden: Vieweg+Teubner Verlag, Springer Fachmedien Wiesbaden GmbH. 738 p.
7. **Yamanaka, T.; Hoshino, H.; Motoyama, K.** 2000. Design optimization technique for suspension mechanism of automobile. Seoul: FISITA World Automotive Congress. Korea Society of Automotive Engineering. Inc. F2000G309.
8. **Hwang, J. S.; Kim, S. R.; Han, S. Y.** 2007. Kinematic design of a double wishbone type front suspension mechanism using multi-objective optimization, Proceedings of the 5th Australasian Congress on Applied Mechanics (ACAM 2007), p. 788-793.
9. **Sancibrian, R.; Garcia, P.; Viadero, F.; Fernandez, A.; De-Juan, A.** 2010. Kinematic design of double-wishbone suspension systems using a multiobjective optimisation approach. Vehicle System Dynamics, International Journal of Vehicle Mechanics and Mobility 48(7): 793-813. http://dx.doi.org/10.1080/00423110903156574.
10. **Arikere, A.; Kumar, G.S.; Bandyopadhyay, S.** 2010. Optimisation of double wishbone suspension system using multi-objective genetic algorithm. SEAL 2010. LNCS 6457. http://dx.doi.org/10.1007/978-3-642-17298-4_48.
11. **Zhang, J. J.; Xu, L.W.; Gao, R.** 2012. Multi-island genetic algorithm optimization of suspension system. Telkomnika 10,7:1685-1691. http://dx.doi.org/10.11591/TELKOMNIKA.V10I7.1563.
12. **Heo, S. J.; Kang, D. O.; Lee, J. H.; Kim I. H.; Darwish, S. M.** 2013. Shape optimization of lower control arm considering multi-disciplinary constraint condition by using progress meta-model method. International Journal of Automotive Technology 14(3): 499-505. https://doi.org/10.1007/s12239-013-0054-7.
13. **Yarmohamadi, H.** 2012. Advances in Heavy Vehicle Dynamics with Focus on Engine Mounts and Individual Front Suspension. Chalmers University of Technology, PhD Thesis, Göteborg. 46 p.
14. **Yarmohamadi, H.; Berbyuk, V.** 2013. Kinematic and dynamic analysis of a heavy truck with individual front suspension. Vehicle System Dynamics: International Journal of Vehicle Mechanics and Mobility 51(6): 877-905. http://dx.doi.org/10.1080/00423114.2013.770539.
15. **Reimpell, J.** 1988. Fahrwerktechnik: Radaufhängungen. 2. Aufl. Würzburg: Vogel Buchverlag. 406 p.
16. **Reimpell, J.; Stoll, H.; Betzler, J. W.** 2001. The Automotive Chassis: Engineering Principles. 2nd Edition. Warrendale: Society of Automotive Engineers, Inc., 444 p.
17. **Montgomery, D. C.** 2000. Design and analysis of experiments. 5th Edition. Hoboken, New Jersey: John Wiley & Sons, Inc. 275 p.
18. **Myers, R. H.; Montgomery, D. C.; Anderson-Cook, C. M.** 2009. Response Surface Methodology, Process and Product Optimization Using Design of Experiments. 3rd Edition. New Jersey: John Wiley & Sons, 704 p.
19. **Topaç, M. M.; Deryal, U.; Bahar, E.; Yavuz, G.** 2015. Optimal kinematic design of a multi-link steering system

for a bus independent suspension: An application of response surface methodology, Mechanika 21(5): 404–413.
http://dx.doi.org/10.5755/j01.mech.21.5.11964.
20. MSC.ADAMS™. 2013. ADAMS/Insight™ User Guide. MSC. Software Corporation.
21. **Aydın, M.; Ünlüsoy, S.** 2012. Optimization of suspension parameters to improve impact harshness of road vehicles, The International Journal of Advanced Manufacturing Technology 60(5-8): 743–754.
http://dx.doi.org/10.1007/s00170-011-3589-7.
22. **Reimpell, J.** 1976. Fahrwerktechnik, Bd. 1, 3. Aufl. Würzburg: Vogel-Verlag.
23. **Blundell, M.; Harty, D.** 2006. The Multibody Systems Approach to Vehicle Dynamics. London: Elsevier Butterworth – Heinemann. 518 p.
24. **Topaç, M. M.; Olguner, C.; Yenice, A.** 2018. Adapter for connection of upper wishbone ball joint and suspension knuckle (Üst salıncak rotil ve akson ara bağlantı adaptörü). Patent No: TR 2015 17648 B. Ankara: Turkish Patent and Trademark Office. 12 p. (in Turkish).
25. **Olguner, C.** 2015. Computer aided design and analysis of a double wishbone suspension for heavy commercial vehicles. Dokuz Eylül University, MSc Thesis, Izmir: 90 p. (In Turkish).

M. M. Topaç, C. Olguner, E. Bahar

DEVELOPMENT OF AN INDEPENDENT FRONT SUSPENSION FOR TRUCK TRACTORS

S u m m a r y

Design and experimental validation stages of an independent front suspension (*IFS*) that is designed for truck tractors of articulated commercial vehicles are summarised. Firstly, the suspension geometry, which satisfies the required conditions of minimum deviation of camber angle and track width during wheel travel, is obtained within the given design volume by using Multibody Systems (*MBS*) and Design of Experiments (*DOE*) approaches. Subsequently, the kinetic analysis is carried out for the suspension system and the critical design loads that may act on the structural elements are determined. Taking these loads into account, the mechanical design of the suspension system elements is performed. The Finite Element Analysis (*FEA*) is applied to the complete suspension system for the chosen critical load conditions. Stress concentrated regions on the crucial system elements are determined and improvements are indicated, which result in the reduction of stress concentrations. In the last part of the study, prototyping and fatigue tests are carried out. Throughout bench tests, in which real service conditions are simulated, no failure of any sort is encountered. The final suspension pair is 31% lighter than an equivalent rigid front axle in terms of load capacity.

**Keywords:** independent front suspension (*IFS*), heavy commercial vehicle, multibody systems (*MBS*), multi objective optimisation, design of experiments (*DOE*), finite element analysis (*FEA*), fatigue.

Accepted May 13, 2021
Received April 08, 2022